J. Phys. B: At. Mol. Phys. **16** (1983) 1633–1656. Printed in Great Britain

Total cross section measurements for positron and electron scattering on molecular hydrogen between 8 and 400 eV

A Deuring†, K Floeder†, D Fromme†, W Raith†, A Schwab†, G Sinapius†, P W Zitzewitz†§ and J Krug‡

† Fakultät für Physik, Universität Bielefeld, D-4800 Bielefeld, Federal Republic of Germany

‡ Institut für Experimentalphysik I, Universität Bochum, D-4630 Bochum, Federal Republic of Germany

Received 9 December 1982

Abstract. An apparatus for the measurement of positron and electron total cross sections on gases is described. The low-energy positrons are produced by moderating high-energy positrons from β-decay sources. We used a ^{11}C positron source, produced at a proton accelerator and, alternatively, a ^{22}Na source, combined with various moderators. For electron measurements the secondary electrons originating from the moderator are used. The beam transport system consists of electrostatic lenses and a weak magnetic lens located in the middle of the gas cell. The discrimination against forward scattering is characterised by a cut-off angle of about 6°. Our e^+–H_2 and e^-–H_2 data are compared with the results of recent measurements of similar accuracy performed at University College London and Wayne State University (Detroit), and with other e^-–H_2 data. The agreement is satisfactory.

1. Introduction

The scattering on H_2 is the most fundamental process in electron/positron scattering on molecules. For that reason this process has been investigated by many experimental groups. Available for comparison with our e^+–H_2 data are the recent results of the London group (Charlton *et al* 1980, Griffith *et al* 1982) and of the Detroit group (Hoffman *et al* 1982). In these experiments electron cross sections were measured as well. Our e^-–H_2 data are also compared with the results of several other experiments which investigated only e^-–H_2 scattering (Golden *et al* 1966, Ferch *et al* 1980, Dalba *et al* 1980, van Wingerden *et al* 1980).

The Detroit group uses a short-lived positron source produced with a proton accelerator and a boron target by the $^{11}B(p, n)^{11}C$ reaction. The boron target also serves as moderator. With this source and moderator Stein *et al* (1975) observed a narrow energy distribution of the moderated positrons with a width smaller than 0.1 eV. In order to separate the low-energy positrons from high-energy positrons a curved solenoid is employed. This magnetic guiding field extends over the whole gas cell and limits the discrimination against forward scattering. Cut-off angles of up to 25° were reported (Hoffman *et al* 1982).

§ Humboldt Fellowship 1979/80. Permanent address: Department of Natural Sciences, University of Michigan, Dearborn, Michigan 48128, USA.

The London group utilises the time-of-flight technique. Previously they used a ^{22}Na source and a MgO-coated tungsten grid moderator (Griffith *et al* 1979). Recently they switched to a tungsten vane moderator. They also employ a magnetic guiding field. Griffith *et al* (1982) quoted a cut-off angle for forward scattering between 5 and 10°.

We built an apparatus with electrostatic 90° deflection of the low-energy positron beam, quite similar to the system developed independently for surface physics studies at Brandeis University (Rosenberg *et al* 1980). To achieve a discrimination against forward scattering which is as good as in our previous TOF experiment (Sinapius *et al* 1980), electrostatic lenses without strong magnetic guiding fields are used for the beam transport. The construction of the apparatus enables us to exploit the advantages of the ^{11}C source produced with a proton accelerator and, alternatively, to use a conventional long-lived positron source at our laboratory. At first we intended to use the ^{22}Na source only for tests and exploratory measurements. The ^{11}C source was thought to be preferable because of its high activity, localised at a small spot, and the narrow energy distribution of the moderated positrons. However, while working with the ^{11}C source we realised several technical problems associated with this method. Target sputtering puts a limit on the usable proton beam current. Different boron samples showed different moderating properties with poor reproducibility. Later, we used the ^{11}C positron source only in conjunction with other, more favourable moderators. In addition we performed many accurate cross section measurements with the weaker ^{22}Na source by automated and computer-controlled long-time data taking.

2. Apparatus

A cross section of the apparatus is given in figure 1; the components of the beam transport system are shown schematically in figure 2. For activation of the boron target located in the source holder, the proton beam enters the apparatus through the two apertures of the beam monitor system (upper left of figure 2). After activation the source holder is rotated through 180° to place the activated target in front of the positron (electron) beam transport system. Alternatively, a ^{22}Na positron source can be used mounted at the same source holder. The electron cross section measurements are made with secondary electrons from the moderator. The low-energy positrons emerging from the moderator are separated from the high-energy positrons and gamma rays by a 90° deflection in a cylindrical mirror spectrometer (CMS). A zoom lens focuses them onto the entrance of the gas cell. A weak magnetic lens is employed to increase the transmission of positrons through the gas cell. Finally, the low-energy positrons are detected by a channel electron multiplier (CEM). The undeflected high-energy positrons pass a hole in the CMS and hit a surface barrier detector (SBD). The gas cell is alternately filled with gas and evacuated. The total cross section is determined from slow-positron counting rates of successive gas and vacuum runs.

2.1. Sources of positrons and electrons

2.1.1. Source holder. The source holder (figure 3) houses up to six boron targets, a Faraday cup for measuring the proton current, and a thermionic cathode for test measurements. A ^{22}Na positron source can also be attached. The source holder is

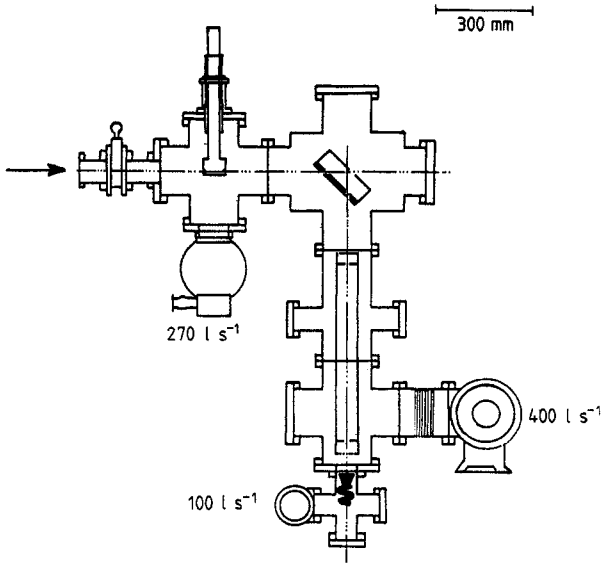

Figure 1. Schematic diagram of the vacuum system.

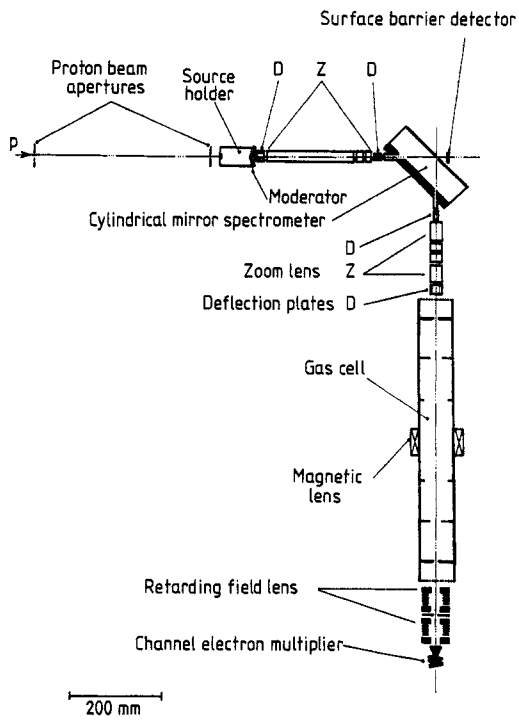

Figure 2. Schematic diagram of the beam transport system.

flanged to a rotatable vacuum feedthrough. It can easily be exchanged. Sealing of the vacuum feedthrough against the atmosphere is accomplished by a Viton-O-ring which allows rotation about and displacement along its vertical axis. The feedthrough

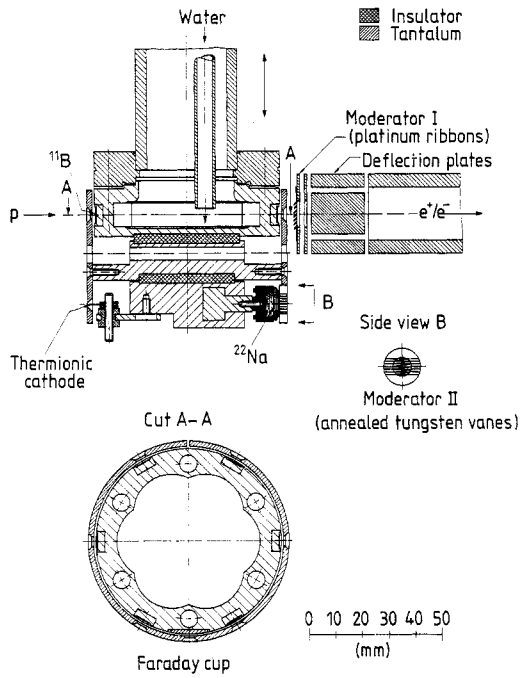

Figure 3. Rotatable source holder and first elements of positron beam transport system. The source holder is shown in the vertical position suited for irradiation of a boron target or the Faraday cup. If the thermal cathode or the ^{22}Na positron source are used the source holder is lifted and moderator I is removed.

is rotated by a remotely controlled motor drive. The whole arrangement is electrically insulated from the rest of the apparatus. Thus the proton current reaching a target or the Faraday cup can be measured by an electrometer inserted between vacuum feedthrough and ground. The energy dumped by the proton beam has to be taken away from the source holder. To enable water cooling the vacuum feedthrough and the source holder are hollow. For optimum heat conduction the source holder is made of copper. The boron targets are vacuum brazed onto the source holder. If copper is accidentally irradiated by protons, two radioactive nucleides are produced: ^{63}Zn and ^{65}Zn with half-lives of 38.4 min and 244 d respectively. Already after only one activation of a boron target (which was done usually for 20–40 min) inadvertent copper irradiation can be detected by monitoring the decay rate of the source. Due to contributions from ^{63}Zn (38.4 min half-life), a slower decrease of the decay rate would be observable than after pure boron activation (20.3 min half-life for ^{11}C). The production of ^{63}Zn with its rather short half-life is not serious, but, if detected, is well suited to avoid a gradual build up of the long-lived ^{65}Zn during repeated activations of the same target. To minimise the chance of copper activation the whole source holder is surrounded by a 2 mm thick tantalum shielding. The tantalum shielding has openings in front of the boron targets and is electrically insulated from the source holder. Thus it can be supplied with a potential suitable to extract low-energy positrons. The Faraday cup consists of a sheet of tantalum (2 mm thick), which is screwed directly onto the source holder. During measurements of the proton current,

the tantalum shielding surrounding the source holder is biased at −200 V to prevent secondary electrons from leaving the irradiated cup.

Originally we thought that it would be possible to activate one boron target while using the previously activated target on the opposite side of the source holder as positron source. This procedure turned out to be impracticable because of background problems. Irradiation of a boron target is accompanied by an increased background counting rate of the channel electron multiplier, although the detector region had been screened by a 100 mm thick lead shielding. Apparently this background is largely due to secondary electrons from gamma radiation.

In the first design we tried to insulate the Faraday cup from the source holder by a sheet of either boron nitride or aluminium oxide. This did not work: at room temperatures both insulators are poor heat conductors. Thus the tantalum sheet and the insulator heated up very quickly during proton irradiation. With increasing temperature, however, the electrical resistance of both materials decreases drastically. Consequently, the Faraday cup was short-circuited to ground potential. Proton beam current measurements with such a cup were possible for only a few seconds. To solve this problem the tantalum sheet of the Faraday cup was mounted directly onto the source holder and the whole vacuum feedthrough was electrically insulated from the rest of the apparatus.

2.1.2. ^{11}C positron source. The ^{11}C decay has a half-life of 20.3 min. It yields fast positrons with a maximum kinetic energy of 0.96 MeV. The (p, n) reaction in ^{11}B starts from a threshold slightly above 3 MeV. From 3 to 7 MeV the cross section rises with some resonant features (Legge and Bubb 1961). We worked with the proton beam of the Dynamitron-Tandem-Laboratorium at the University of Bochum. A proton beam current of up to 100 μA was available at energies up to 8 MeV. For measurements on-line we had a total of 14 d in 1980/81/82.

The proton beam is focused onto a boron target with the aid of the beam monitor system (figure 4). It consists of two water-cooled apertures and the Faraday cup mounted in the source holder. The second aperture is divided into electrically insulated quadrants for determining horizontal and vertical deviations of the beam. Relative current measurements are possible on each of the apertures. The proton beam has a core of high current density surrounded by a halo. From measurements with

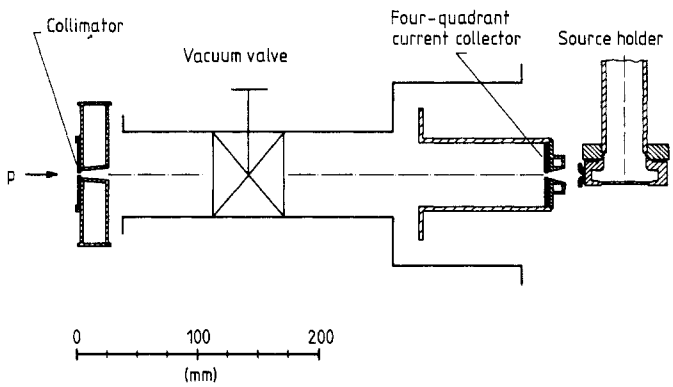

Figure 4. Proton beam monitor system.

source-holder rotation (cf § 3.1.1) the proton beam diameter was estimated to be approximately 1.5 mm.

Calculations were made in order to determine the optimum proton energy for the ^{11}C production and the required target thickness. For the β-decay positrons we estimated the probability of escape from the boron.

To evaluate the ^{11}C production rate, the path of the protons has to be traced through thin slices of boron, taking into account the energy loss of the protons. The production rate was obtained as a weighted sum of energy-dependent rates. The energy loss for protons may be calculated with an approximate form of the Bethe formula (Livingston and Bethe 1937):

$$-dE/dx = 4\pi NZe^4(mv^2)^{-1}\ln(2mv^2/I). \tag{1}$$

This approximation holds if the proton energy E satisfies:

$$(M/m)I \ll E \ll Mc^2. \tag{2}$$

The symbols used have the following meanings: c, is the velocity of light; e, the electron charge; m, the electron mass; M, the proton mass; v, the proton velocity; N, the number density of atoms in the target material; Z, the nuclear charge of the target atoms and I, the average ionisation energy of the target atoms.

In the calculations a boron density of 2.34 g cm^{-3} and an approximate value of 70 eV for the average ionisation energy were used. The results have an accuracy of about 10%. The expected ^{11}C activity after one half-life of activation with a proton current of 1 μA is shown in figure 5. Using equation (1) the proton ranges listed in table 1 were derived. The activation depth is about 0.08 mm less than the range given in table 1 because protons below activation threshold do not contribute to the activation.

At higher energies more of the ^{11}C is produced deeper inside the boron. Consequently, some positrons are stopped and annihilated before reaching the surface.

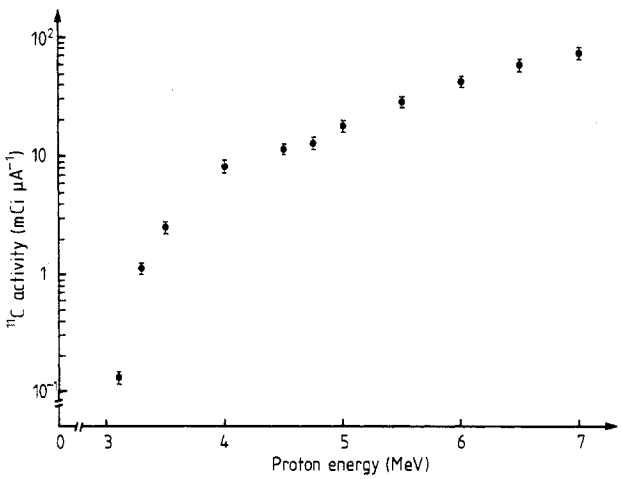

Figure 5. ^{11}C activation in the $^{11}B(p, n)^{11}C$ reaction as a function of the proton energy. The ^{11}C activity after an activation time t_A of $\tau_{1/2}$ (20.3 min) is given in units of mCi μA^{-1} of proton current. The values have an accuracy of 10%.

Table 1. Proton range in boron and escape probability for the positrons from the boron for different activation energies (last digit uncertainty in parentheses).

Proton energy (MeV)	Proton range (mm)	Escape probability
4	0.13 (1)	0.88 (13)
4.75[a]	0.17 (2)	0.80 (12)
5	0.19 (2)	0.78 (12)
6	0.26 (3)	0.74 (11)
7	0.34 (3)	0.66 (10)

[a] 4.75 MeV is the proton energy used by the Detroit group.

By using data for electron ranges in matter the fraction of positrons stopped can be estimated. For convenience in computing we used the analytical expression for $R(E)$ for electrons given in *Nuclear Engineering Handbook* (1958). In order to evaluate the escape probability of the positrons (table 1) we averaged over their emission depths, energies, and angular distributions and compared their path lengths to the surface with the computed ranges. Due to the neglect of annihilation in flight as well as the uncertainty of the electron and positron ranges at low energies all those values may be affected by systematic errors of about 15%.

The most severe technical problem in the activation is the heat transport away from the boron. At room temperature boron has a poor thermal conductivity. To prevent it from melting, thin targets brazed onto a material with a good thermal conductivity are necessary. A lower limit for their thickness is given by the proton range calculated above (table 1). To keep the thermal strain of the boron targets low, higher activation energies are favourable. Due to the faster than linear increase of the ^{11}C production with rising proton energy (figure 5), the energy transfer to the boron per produced mCi of activity decreases. The increase in activity outweighs the reduced positron emission probability. A proton energy of 7 MeV and a boron thickness of 0.25–0.35 mm seem to be best.

Two kinds of boron targets were tested. Initially we used boron powder (98.5% of ^{11}B, supplied by Oak Ridge National Laboratory), pressed into form with 12 tons cm^{-2} and sintered at about 600 °C in order to achieve mechanical stability. It formed a very hard, glass-like surface, presumably due to B_2O_3 formation. These targets were easy to prepare but apparently their density was lower and their thermal conductivity poorer than that of targets cut from bulk material. Therefore, we switched to polycrystalline targets made from 5 mm diameter rods (99.9995% boron, supplied by Koch-Light Laboratory). These rods were cut into 0.1–0.4 mm thin slices with a diamond saw. We experimented with different thicknesses. The boron slices were attached to the source holder in two steps employing vacuum brazing: (1) brazing of boron to copper support discs with a solder having a high melting point, (2) brazing the discs to the source holder using solder with a lower melting point.

2.1.3. ^{22}Na positron source. This positron source was manufactured by Amersham Buchler and consists of 5 mCi of ^{22}Na deposited as a 3 mm spot on a platinum substrate. It is sealed with a titanium foil window (5 μm thick). The source is inserted either into a holder mounted below the ^{11}C sources (see figure 3) or into a special support flanged to the rotatable vacuum feedthrough instead of the ^{11}C source holder.

2.1.4. Electron sources. The thermionic cathode, mounted on the source holder as shown in figure 3, was initially used for tests of the electron optics, which required measuring currents at various elements of the beam transport system. For the electron cross section measurements, however, we chose the secondary electrons originating from the moderator. In this way no mechanical variations of the apparatus are necessary to switch from positron to electron measurements. The size of this electron source and the angular distribution of the electrons emitted are quite similar to those of the positrons. The secondary electron counting rate exceeds that of the moderated positrons by about a factor of 150 and proved to be sufficiently stable.

One disadvantage of using secondary electrons is their broad energy width of about 2–2.5 eV (FWHM). This energy distribution is acceptable for cross section measurements if the cross section varies slowly with energy. Below 20 eV, however, the e^-–H_2 cross section changes rapidly with energy. Therefore, we used the retarding potential of the filter lens to cut the low-energy tail of the distribution at two different cut-off energies E_1 and E_2 separated by 1 eV. The difference of the counting rates can be attributed to electrons with energies between E_1 and E_2 (with this energy interval smeared out by the energy width of the filter lens).

2.2. Moderators

During the first accelerator runs we used the boron itself as a moderator, following Stein *et al* (1974). Because they reported an increased yield of low-energy positrons from oil contaminated boron (Stein *et al* 1975, Pendyala and McGowan 1980), we tried (unsuccessfully) to obtain a higher yield in a similar way. A small tube with a 0.1 mm diameter hole was filled with organic diffusion pump oil and placed at a distance of 80 mm from the boron targets.

We later used venetian blind moderators as shown in figure 3 in conjunction with the ^{11}C and also with the ^{22}Na source. The platinum moderator was fabricated out of a 0.02 mm thick platinum foil by making parallel cuts, 5 mm long and 2 mm apart. The resulting ribbons are twisted by 45°. The optical transmission is about 30%. Stimulated by the work of Dale *et al* (1980) we also used tungsten as the moderator, trying various cleaning and annealing procedures. This is made out of 0.25 mm thick and 2 mm broad ribbons, mounted parallel to the beam axis. The optical transmission is about 75%. The ribbons were annealed at temperatures above 1600 °C at 10^{-5} Torr before mounting.

2.3. Positron beam transport system

An electrostatic beam transport system was chosen to provide good discrimination against forward scattering in our cross section measurements. However, the transmittance of such a system, if used with extended sources emitting particles with a broad energy distribution into a large solid angle, is much lower than in systems employing magnetic guiding fields.

Our system (figure 2) was designed to transport a beam of slow positrons (electrons) from the moderator through the gas cell to the detector and to separate the moderated positrons from the high-energy positrons and the gamma rays. The first electron optical component beyond the moderator is a zoom lens, followed by a cylindrical mirror spectrometer. In its electrostatic field the slow particles are bent through a 90° angle towards the gas cell. The following zoom lens focuses the positrons onto

the entrance of the gas cell. Deflection plates are installed at both ends of the zoom lenses to compensate for beam deviations due to residual magnetic fields and misalignment of the optical components. A retarding field lens is located between the gas cell and the detector. The design of the zoom lenses is based on the diagrams of Harting and Read (1976). Electron trajectories through the whole system were computed by using the program of Herrmannsfeldt (1973). The components of the beam transport system are made of non-ferromagnetic stainless steel or copper.

The cylindrical mirror spectrometer (CMS) is constructed as described by Risley (1972). The resolvable energy ΔE_{CMS} is proportional to the energy E of the particles entering the CMS and also depends on the diameters of the entrance and exit apertures and the diameter and angular divergence of the positron beam. For most of the cross section measurements high intensity was more important than a reduced energy width, therefore the cylindrical mirror spectrometer was only used for the 90° beam deflection, not as an energy monochromator. For maximum transmission the spectrometer was operated with wide apertures and at a high transmission energy of 50 to 250 eV. Under these conditions ΔE_{CMS} is larger than the energy width of the particles from the moderator. Only for the special purposes of testing the energy resolution of the retarding field lens (as described in § 2.5), and determining an upper limit for the energy width of the slow positrons emitted from the boron, did we use the CMS as an energy analyser.

2.4. Gas cell

The gas cell is a 515 mm long, 67 mm diameter tube with 3 mm apertures at both ends (figure 2). A weak magnetic lens images the entrance onto the exit aperture. Both the gas inlet and the ionisation gauge pipes are welded to the wall of the gas cell close to the middle of the tube. The ionisation gauge was calibrated with a capacitance manometer. In order to avoid unknown contact potential differences between the retarding element of the retarding field lens (made of copper) and the gas cell, the interior of the cell is lined with a copper mesh. Four copper apertures are inserted. They reduce the chance that positrons (electrons), removed from the beam by a collision with a gas particle, reach the detector via collisions with the wall. The maximum entrance angle for particles to pass the cell is 3.7°. From this angle and the design parameters of the cell the cut-off angle for forward scattering was calculated to 6° averaged over the whole length of the cell.

The target gas density $n(z)$ has non-negligible values in the regions adjacent to the gas cell (between z_1 and z_2 in figure 6(a)). By the design shown in figure 7 it was ensured that the energy of the positrons (electrons) in those regions is the same as inside the cell.

For accurate scattering measurements identical pressure conditions in the beam transport system are necessary during the measurements without and with gas. To achieve this, a by-pass is mounted which, during measurements without gas, directs the gas flow to the entrance and exit regions of the gas cell. The gas supply is shown in figure 8.

In our data evaluation we use the product $n(z_0)L_{eff}$, where $n(z_0)$ is the measured number density of the target gas particles in the middle of the gas cell and L_{eff} is the effective length of the scattering region, defined by

$$L_{eff} = n(z_0)^{-1} f \int n(z)\,dz. \tag{3}$$

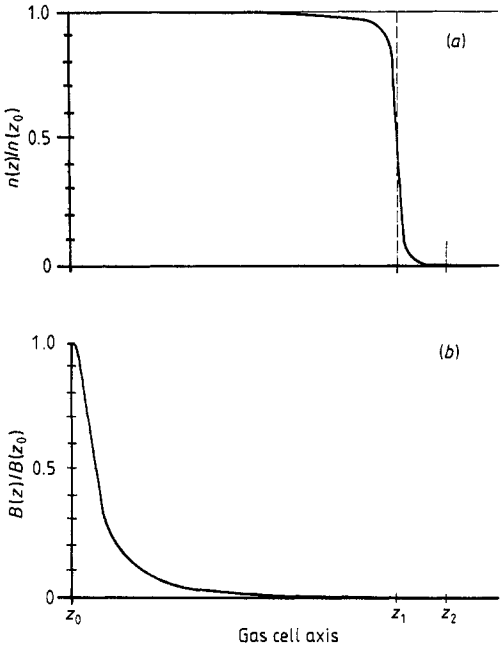

Figure 6. (*a*) Normalised density distribution of the target gas along the z axis of the gas cell. z_0 defines the centre of the cell, z_1 the aperture and z_2 the exit mesh ($z_0 = 0$ mm, $z_1 = 257.5$ mm, $z_2 = 300$ mm). (*b*) Relative strength of the axial component of the field of the weak magnetic lens along the axis: $B(z)/B(z_0)$. $B(z_0) = 4.2$ G for positrons with an energy of 10 eV.

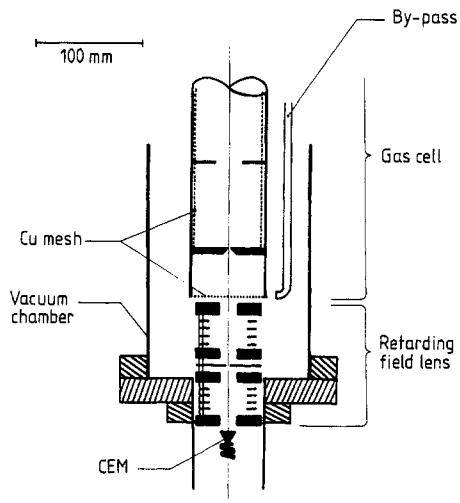

Figure 7. Scattering region and retarding field lens.

In this expression the integral extends between $-z_2$ and $+z_2$ (figure 6(*a*)); $n(z)$ is the number density along the axis and f is the factor which takes into account the average lengthening of the trajectories due to the field of the magnetic lens (figure 6(*b*)). The trajectory length of a particle in the cell is a function of its entrance angle. We

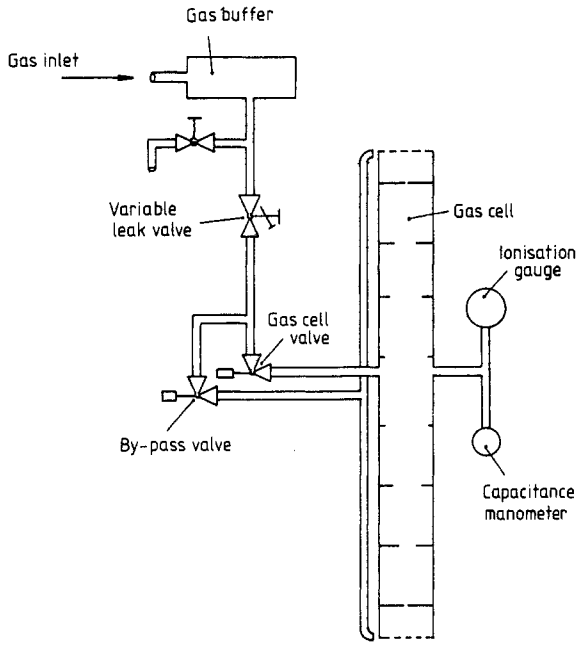

Figure 8. Gas handling system.

evaluated the integral of equation (3) using the function $n(z)$ shown in figure 6(a), and then calculated $L_{\text{eff}} = 518(5)$ mm.

2.5. Retarding field lens

The lens (figure 7) is an adaption of the design described by Simpson (1961). The retarding electrode has a hole of 5 mm diameter, covered with a 200 wires/in copper mesh (78% transmission). To minimise the distortion of the electric field inside the lens due to the grounded walls of the vacuum system, four copper rings are installed between the outer pairs of lens elements. They are supplied with the appropriate intermediate potentials.

The main purposes of the retarding field lens are to calibrate the origin of the positron (electron) energy scale and to truncate the energy distribution of the electrons for scattering measurements at low energies as described in § 2.1.4.

The theoretically resolvable energy of the lens depends on the angular spread of the incoming beam (Simpson 1961) according to

$$\Delta E_{\text{RFL}} = EM^{-2} \sin^2 \theta. \tag{4}$$

In this expression E denotes the energy of the incoming particles, M the magnification of the lens ($M = 1.11$ for our design and voltage ratios), and θ the maximum angle between the optical axis and the direction of the incoming particles, about 9° in our case. According to equation (4) the retarding field lens should have a resolvable energy of $\Delta E_{\text{RFL}} = 0.02E$.

An experimental value for the resolvable energy of the lens was obtained in the following way: the cylindrical mirror spectrometer was operated as a monochromator.

Varying the transmission energy of the CMS, electron beams with different energy widths were selected from the incident secondary electrons. They were transmitted through the gas cell at different energies. For each combination of CMS and gas cell transmission energies the energy distribution was analysed with the retarding field lens, operated at appropriate potentials. The energy width measured with the retarding field lens is the energy width of the electron beam folded with the energy resolution function of the lens. (The magnetic lens in the middle of the gas cell has no influence on the energy distribution of the analysed beam.) From the measurements we derived an experimental value $\Delta E_{\mathrm{RFL}}(\mathrm{FWHM}) = 0.02E$ (where E is the energy of the electrons entering the lens) for the resolvable energy in reasonable agreement with the value mentioned above.

2.6. Particle detectors

High-energy positrons traversing the cylindrical mirror spectrometer through a hole in the outer cylinder are detected by a silicon surface barrier detector (SBD). Thus the positioning of the positron source and its activity as a function of time are monitored. The detector is suited to detect positrons with energies ranging from 30 to 6000 keV.

For the detection of the low-energy positrons (electrons) a channel electron multiplier (CEM) is used. The cone of the multiplier is biased at −200 V (+200 V for electrons) compared with the ground potential.

2.7. Compensation of the Earth's magnetic field

The whole apparatus is surrounded by three orthogonal pairs of compensation coils. Because of inhomogenities in the local magnetic field and imperfect compensation by these large coils two additional pairs of coils are installed close to the gas cell for fine adjustment, and a single coil is located behind the cylindrical mirror spectrometer.

For each pair of coils coarse adjustment of the current is achieved by measuring the magnetic field at the apparatus with a magnetometer probe and choosing the current appropriate to minimise the field. Fine adjustment is accomplished by tuning the currents for maximum counting rate at the channel electron multiplier. This tuning has to be iterated several times because the tuning parameters are not fully independent.

2.8. Vacuum system

The vacuum system (figure 1) is made out of stainless steel components. Copper gaskets are used to achieve bakeability. Because of its Viton-O-ring the rotatable vacuum feedthrough can only be baked mildly. The system is evacuated by three turbomolecular pumps. Typically we achieve pressures of about 10^{-7} to 10^{-8} Torr with the gas inlet closed. With 10^{-3} to 10^{-4} Torr in the gas cell (typical pressures for scattering measurements) the pressure in the gas surrounding the cell rises to 10^{-6} Torr.

2.9. Data aquisition

The data aquisition is controlled with a microcomputer. For flexibility and ease of programming we use a DEC LSI-11. The interaction with the experiment goes via

a crate system which contains DAC, ADC, a clock, a counter, and several 16 single-bit input/output channels. The LSI is equipped with a teletype and two cartridge tape drives. The program is written in Fortran on a PDP-11 computer from where an executable version is copied on a cartridge tape.

The counts with and without gas in the gas cell, the CEM dark counts, the respective counting times, and the pressures with and without gas in the cell are recorded on cartridge tape. The data are then further processed on a PDP-11. For runs with the ^{11}C positron source the appropriate corrections for the decay time are applied.

Originally we also intended to use the computer for beam optimisation after changes in energy. This, however, turned out to be a problem of too many parameters to be easily handled by a computer. We used it, however, to optimise up to three parameters when we tested the system prior to the actual measurements.

3. Experiences and results

3.1. Boron targets

3.1.1. Measurements during activation. In order to control the position of the rotatable source holder an analog position monitor was incorporated. However, we found that the positioning of the source holder could be controlled even better by utilising the following observations. If the source holder is rotated during the proton bombardment and the components of the beam transport system are supplied with potentials for electron transport, the counting rate of the channel electron multiplier increases sharply whenever the proton beam hits an edge of an opening in the tantalum shield surrounding the source holder (figure 9). The increase in the counting rate is most probably caused by protons that are scattered sideways from the edge and produce secondary electrons which reach the first zoom lens after wall collisions. If, however, the protons are incident normal to the tantalum surface, they are mainly scattered backwards to the second aperture of the beam monitor system, from where secondary electrons are less likely to reach the electron multiplier. In this case the counting rate is low. When a boron target or the Faraday cup is hit, the electron multiplier counting rate is even lower, because a number of the scattered protons hit the back of the tantalum surrounding the source holder, from where hardly any electrons can get out. The position of the source holder can also be monitored with the surface barrier detector. Its counting rate increases when the proton beam hits the boron (figure 9). Apparently this is due to the neutrons produced in the (p, n) reaction. When they hit the silicon in the surface barrier detector, presumably protons from Si(n, p)Al reactions give rise to a signal. Finally, the activation of the boron is also indicated by the neutron flux meters installed near the apparatus.

Measurements, as described above, are suited to determine the profile of the proton beam. For that purpose the counting rates of the surface barrier detector (SBD) and the electron multiplier are recorded during a slow motor driven rotation of the source holder. The horizontal width of the proton beam was determined by comparing the widths of the maxima measured with the SBD and the widths of the minima between two neighbouring peaks of the secondary electron counting rate of the CEM with the diameter of the aperture in front of the boron target. The vertical width of the beam was estimated in a similar way and also by measuring the width of the traces which the proton beam smelted into some of the boron targets and into

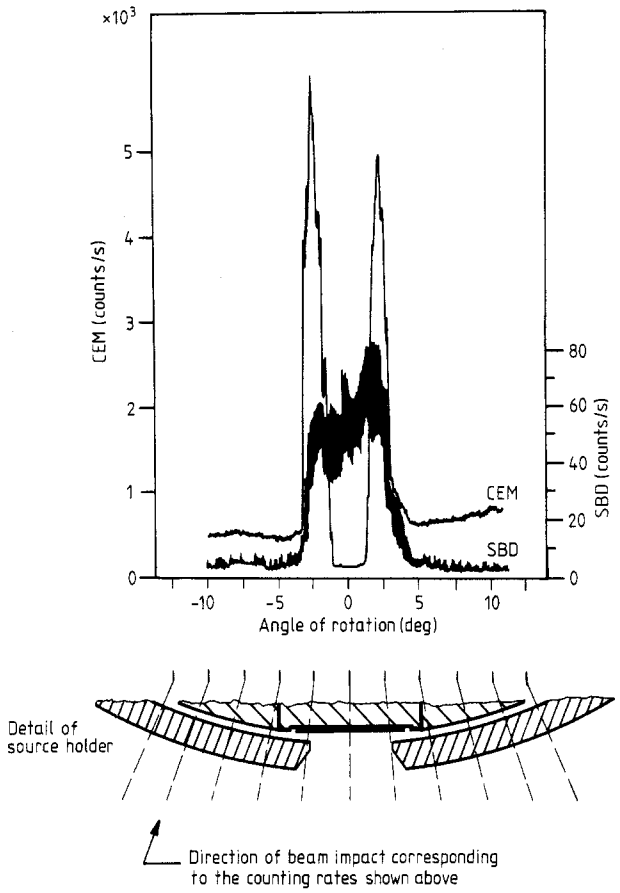

Figure 9. Counting rates of CEM (due to secondary electrons) and SBD (presumably due to protons from Si(n, p)Al reactions) plotted against the position of the source holder during proton bombardment. For comparison a cut through the tantalum shield and a boron target is shown below the diagram. The target facing the zoom lens had not been activated before these measurements. Thus it did not contribute to the counting rates.

the tantalum surface. From those measurements we conclude that the proton beam at the boron target was concentrated in a spot of 1.5 mm diameter.

3.1.2. Activation yields. From the calculations described in § 2.1.2 followed an optimum target thickness of less than 0.4 mm. First tests at the accelerator showed that the targets were damaged by sputtering due to proton impact. To increase the useful life of the targets, boron slices thicker than the calculated values were used. With about 30 μA of 5 MeV protons a fast destruction of the targets was observed. By using a higher proton energy and a lower current (cf figure 5) higher activations could be achieved with significantly reduced target damage. To further reduce target damage it would have been desirable to either defocus or scan the proton beam over a target area of 4 mm diameter; for technical reasons this was not possible in the time available to us. In general we worked with a beam diameter of about 1.5 mm. With these limitations activities between 200 and 300 mCi were usually produced.

The target activity was measured with the SBD and compared with the activity calculated in accordance with § 2.1.2. In all the runs the measured activity was less than estimated; we typically measured only about 40% of the calculated value. Stein *et al* (1974) quoted an activity of 45 mCi for 10 μA of 4.75 MeV protons and an activation time of 45 min. This reflects a similar discrepancy.

3.2. Properties of the moderators

Before measuring the cross section we studied the moderation properties of boron: the yield and the energy distribution of the low-energy positrons. The CEM was mounted below the second zoom lens. We define the yield as the ratio of the low-energy positron rate divided by the β^+ activity of the source. Since this yield definition includes the transmittance of our beam transport system it is smaller than the conversion efficiency defined by Canter and Mills (1982).

Large variations in the yield were observed for different targets and consecutive activations. In some cases no low-energy positron was found. Good boron moderators had a yield of about 10^{-7}, in agreement with the yield quoted by Stein *et al* (1974).

The energy width of the boron moderated positrons was investigated with the CMS. For fixed potentials at the inner cylinder (i.e. positron energies) we varied the outer cylinder potential continuously. From the recorded low-energy positron rates we determined the apparent energy widths (figure 10), which are the positron energy widths folded with the resolution function of the CMS. According to Risley (1972) the energy resolution of the CMS is given by the slope of the broken line in figure 10. It amounts to 4.5% of the entrance energy of the positrons. From figure 10 we furthermore determined the energy width of the positrons to be smaller than 0.5 eV; Stein *et al* (1975) quote a value smaller than 0.1 eV.

As described in § 2.2 we tried to increase the yield by oil contamination. However, we did not find a significant effect during the two days the oil tube was inside the apparatus. Therefore we installed tungsten and platinum vane moderators. These

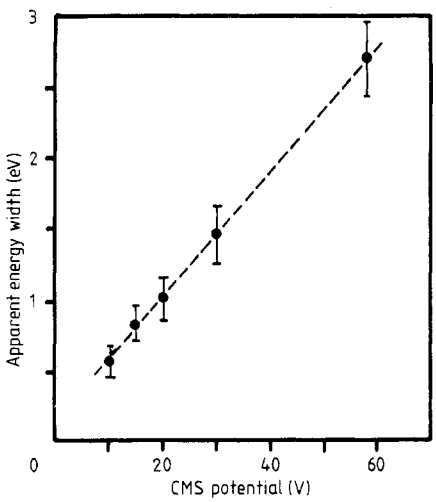

Figure 10. Energy width (FWHM) of transmitted boron-moderated positrons as a function of their mean energy (defined by the CMS potential). The broken line shows a least squares fit.

moderators were also used together with the ^{22}Na source. We observed a yield of about 3.5×10^{-6}.

3.3. Total cross section measurements on H_2

3.3.1. *Determination of cross sections.* For each pair of successive measurements without and with gas in the cell (counting rates R_0 and R respectively) the total cross section Q is determined from the ratio of the counting rates according to the equation

$$Q = (n(z_0)L_{\text{eff}})^{-1} \ln(R_0/R) \tag{5}$$

where $n(z_0)$ is the number density of the scattering gas in the middle of the gas cell and L_{eff} is the effective length of the scattering region evaluated in § 2.4. The counting rates R_0 and R are corrected for the background counting rate.

For the electron measurements below 20 eV data were taken with two different filter lens settings in order to narrow the energy distribution as explained in § 2.1.4. By taking the difference of two counting rates as the signal of the electrons in the selected energy interval, the deduction of the background counting rate is automatically implemented. For the positron measurements this method was not used because of insufficient intensity.

At each particle energy up to 60 measurements of R_0 and R were performed. The counting times were chosen sufficiently long to keep the statistical error of each value for Q obtained according to equation (5) below 5%; in most cases this error is less than 2%. The target gas pressure was varied frequently to ensure that the cross sections obtained are independent of pressure. Typical results are shown in figure 11. The individual measurements of Q were checked to be distributed around the mean as expected for the appropriate Gaussian distribution.

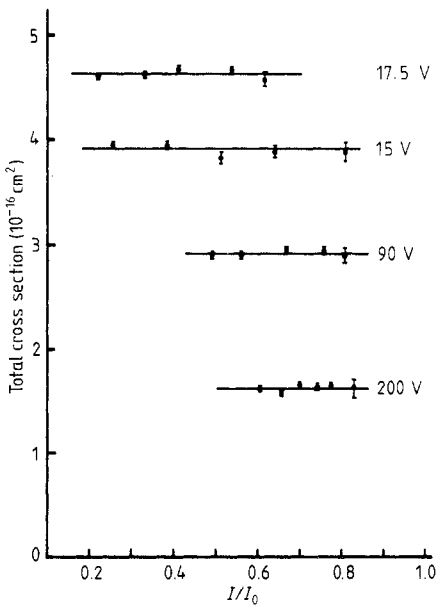

Figure 11. Measured e^+–H_2 cross sections plotted against beam intensity attenuation (I/I_0). The pressure range is 0.3–2.0 mTorr.

The final value for Q at a given particle energy is computed by taking the weighted mean of all these values, with the weight of each value being inversely proportional to the square of its statistical error. The error of Q as shown in figures 12, 13, and 15 and listed in the appendix is the weighted RMS deviation of the individual measurements and takes into account all uncorrelated fluctuations.

3.3.2. Systematic errors. The sources and magnitudes of systematic errors are listed in table 2. The total systematic error has to be added to the error bars of figures 12, 13, and 15 and to the errors of the cross sections listed in the appendix.

Table 2. Sources and magnitudes of systematic errors.

Source of systematic error	Error (%)
Capacitance manometer	1
Pressure calibration	2
Geometric length of gas cell	0.5
Calculation of gas density distribution	0.5
Calculation of mean trajectory length in gas cell	1
Total absolute systematic error	5

The energy width (FWHM) of our positrons, of up to 1 eV, and electrons, of 2–2.5 eV, above 20 eV and (with the filter lens used as mentioned in § 2.1.4) approximately 1 eV up to 20 eV prevents us from resolving small structures. Examples are the sudden increase of the positron cross section at the threshold for H_2 ionisation resolved by the London and Detroit measurements. Additionally, the energy width of the projectile particles introduces a certain error into our results. This error is due to the fact that equation (5) is strictly valid only for measurements performed with a monoenergetic beam. If the particle beam has a normalised distribution $\eta_0(\varepsilon)$ centred at an energy E, the total scattering cross section has to be evaluated by considering the equation

$$R(E)/R_0(E) = \int \eta_0(\varepsilon) \exp(-Q(\varepsilon) n(z_0) L_{\text{eff}})\, \mathrm{d}\varepsilon. \tag{6}$$

The energy distribution $\eta_0(\varepsilon)$ is not known. For an estimate we presumed a Gaussian distribution in connection with the energy width quoted above, and supposed the cross section to vary linearly over an energy range larger than the energy width. The differences between the cross sections sufficing equation (6) and those values obtained using equation (5) are negligible (smaller than 0.5%).

Because of the good discrimination against particles scattered in the forward direction (the cut-off angle is about 6°, corresponding to a solid angle of only $\Omega/4\pi = 0.003$) the error introduced into the measured cross sections by detection of scattered particles is rather small. As no differential scattering information is available the amount by which the cross sections are too low cannot be estimated.

3.3.3. Positron measurements. Our values of the total cross sections for positrons scattered on molecular hydrogen are presented in figures 12 and 13. As there are no systematic deviations between measurements with the ^{11}C positron source at the

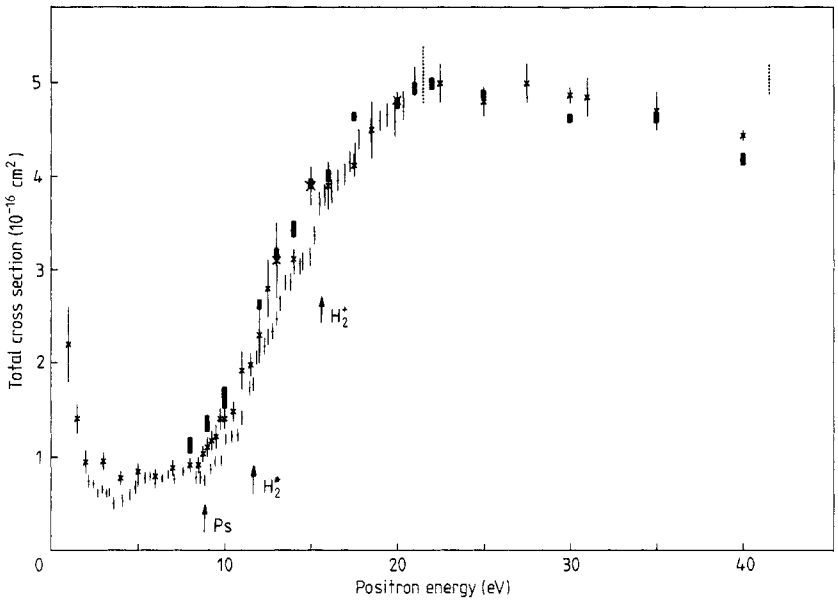

Figure 12. Total e^+–H_2 scattering cross section measurements below 42 eV. The error bars represent the statistical errors. The thresholds for positronium formation, electronic excitation, and ionisation are indicated by arrows. Results: ⁝, Charlton *et al* (1980) (London); ⁞, Griffith *et al* (1982) (London); ×, Hoffmann *et al* (1982) (Detroit); ■, present results (Bielefeld).

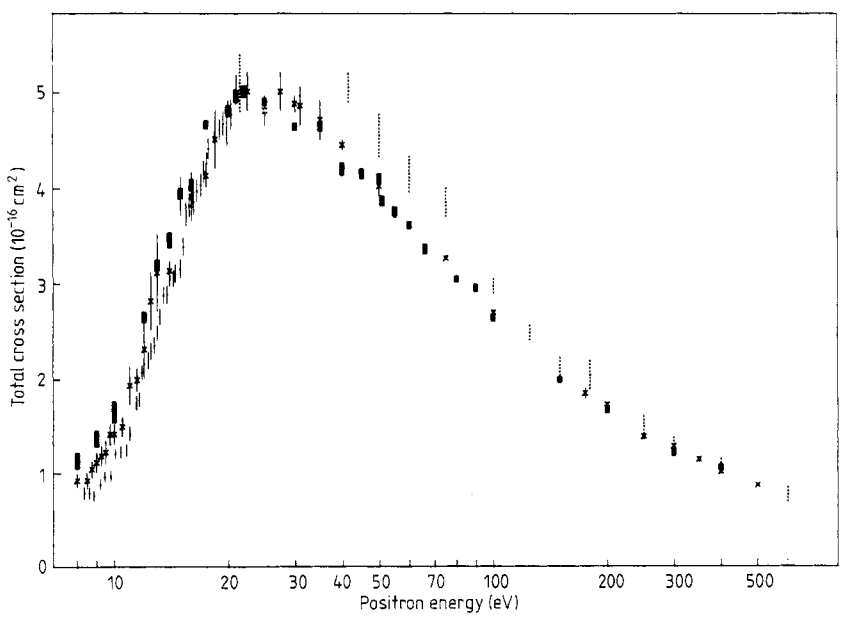

Figure 13. Total e^+–H_2 scattering cross section measurements between 8 and 600 eV. Otherwise, same as for figure 12.

accelerator and those taken with the ^{22}Na positron source, the cross sections were evaluated from all available data (as described in § 3.3.1). The most recent results reported by the London group (Charlton *et al* (1980) and Griffith *et al* (1982), superseding any previously published data of this group) and the Detroit group (Hoffman *et al* 1982) are included.

Figure 12 shows the results at low energies. Each of the three sets of measurements shows a sharp increase in the cross section above the threshold for positronium formation (8.73 eV), above which other inelastic processes also contribute to the total cross section. In the energy range from 8 eV to about 18 eV our results are higher than those of both the other groups. The averaged difference between our measurements and the Detroit and London measurements is 10 and 19% respectively. Taking into account the total errors, however, our results do not contradict the Detroit data (cf figure 14 and table 3). Possibly, the discrepancies in the 8–18 eV energy range do not result from systematic errors in the cross section measurements but rather from errors in the absolute positron energy scale. The discrepancy between the Detroit and Bielefeld data would disappear almost entirely if an energy shift of about 1 eV

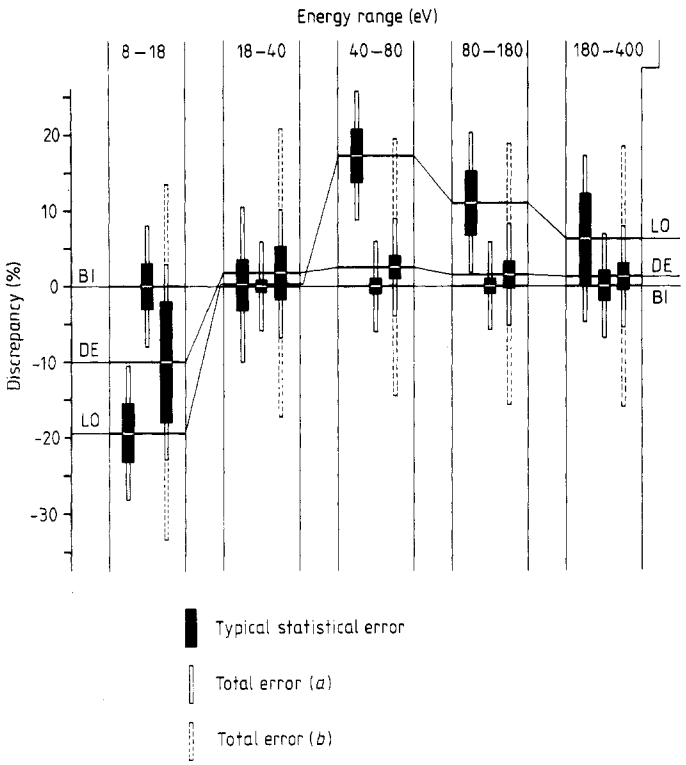

Figure 14. Comparison of the total e^+–H_2 scattering cross sections measured by different groups, considering their statistical and systematic errors. Results: LO, Charlton *et al* (1980), Griffith *et al* (1982) (London); DE, Hoffman *et al* (1982) (Detroit); BI, this work (Bielefeld). The results for selected energy intervals were averaged and our data taken for normalisation. The total error is the sum of errors given in table 3. For the Detroit results (*a*) includes the 'experimental errors' and (*b*) the 'maximum errors' as quoted by these authors. (Note: the deviations in the lowest energy range might possibly be caused by errors in energy scale.)

were applied to either data set. The discrepancy between the London and Bielefeld data corresponds to an energy offset of about 1.7 eV. The different cut-off angles for forward scattering (table 3) might also account for some of the differences, but do not explain the distance between the results of the London and Bielefeld experiments, which both have small cut-off angles.

In figure 13 the cross section results up to 600 eV are presented on a logarithmic energy scale. At higher energies our results differ from the Detroit measurements by 1–6% only, which is compatible with the statistical errors. The London data between 40 and 80 eV are consistently higher with discrepancies of up to 22% compared with our measurements. For a detailed comparison of the data sets and the errors of those measurements we refer the reader to figure 14.

There are no theoretical calculations available for total e^+–H_2 scattering cross sections. The calculations of Baille *et al* (1974), Darewych *et al* (1974), Hara (1974), and Bhattacharyya and Ghosh (1975) consider elastic scattering only. They can be compared with the total cross section measurements only for energies below the positronium formation threshold. The calculations of Hara (1974) and Bhattacharyya and Ghosh (1975) agree satisfactorily with the measurements; the results of Darewych *et al* (1974) and Baille *et al* (1974) are lower.

Table 3. Errors attached to the e^+–H_2 results of the different groups.

Group	Typical statistical error[a] (%) Energy range (eV) 8–18	18–40	40–80	80–180	180–400	Additional random errors (%)	Systematic errors (%)	Cut-off angle for forward scattering[b] (deg)
Charlton *et al* (1980) (London)	—	5.3	3.5	4.2	6.1	3[c]	2[c]	5–10[d]
Griffith *et al* (1982) (London)	3.9	2.8	—	—	—	3[c]	2[c]	5–10[d]
Hoffmann *et al* (1982) (Detroit)	8.0	3.4	1.4	1.7	1.6		5[e] 15.5[f]	9–25
Present results (Bielefeld)	2.9	0.8	1.0	0.9	1.9		5	6

[a] cf § 3.3.1 for our results.
[b] Resulting error not included in the systematic errors.
[c] Quoted by Griffith *et al* (1979).
[d] Quoted by Griffith *et al* (1982).
[e] 'Experimental error' as quoted by the Detroit group.
[f] 'Maximum error' as quoted by the Detroit group.

3.3.4. Electron measurements. The measured electron cross sections on H_2 are presented in figure 15. For comparison we include the data quoted by the London group (Griffith *et al* 1982) and the Detroit group (Hoffman *et al* 1982) as well as the results reported by authors who carried out electron measurements only (Golden *et al* 1966, Ferch *et al* 1980, Dalba *et al* 1980, and van Wingerden *et al* 1980). The very early measurements of Rusch (1925), Brode (1925), Brüche (1927), Ramsauer and Kollath (1930), and Normand (1930) are not shown.

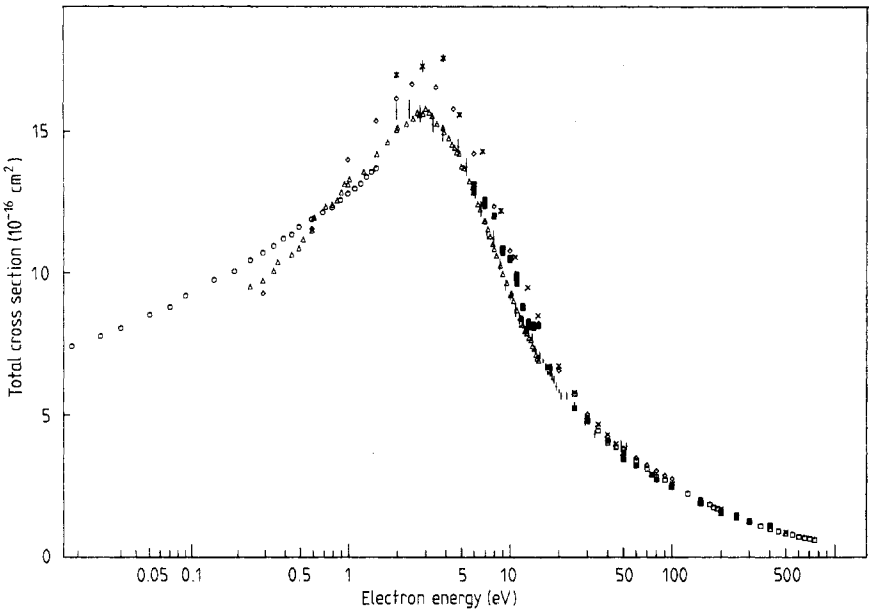

Figure 15. Total e^-–H_2 scattering cross section measurements. The data of London, Detroit, and Bielefeld groups are shown with the statistical errors. The systematic errors quoted by these groups are the same as for the positron measurements (table 3). Van Wingerden *et al* (1980) estimate a statistical error of 1%, which is smaller than the dots. The other results are given without error bars, because the authors do not quote statistical and systematic errors separately. Golden *et al* (1966) quote a total error of 3%, calculated as the square of the quadratic sum of the different errors. Dalba *et al* (1980) compute the 'overall error' in the same way; it varies with the electron energy between 1.7 and 7%. Ferch *et al* (1980) claim an accuracy of 2.5% taking into account statistical as well as systematic errors. Van Wingerden *et al* (1980) take the absolute sum of the single errors as their total error (3.1% below 100 eV and 3.4% above 100 eV). Results: |, Griffith *et al* (1982) (London); ×, Hoffmann *et al* (1982) (Detroit); ■, present results (Bielefeld); △, Golden *et al* (1966); ○, Ferch *et al* (1980); ◇, Dalba *et al* (1980); □, van Wingerden *et al* (1980).

At energies above 15 eV the plotted cross sections of all the groups agree within the total errors. Systematic deviations exist in the energy range below 15 eV, where the difference between the highest and the lowest measurements exceeds the uncertainties given by the total errors.

In contrast to the positron measurements, where the Detroit results are consistently lower than our data below 18 eV, nearly all the Detroit e^-–H_2 cross sections are a little higher than our measurements. The London data of Griffith *et al* (1982) are the lowest results for both positron and electron cross sections in the whole energy ranges covered by them.

The theoretical results of Wilkins and Taylor (1967), Hara (1969), Henry and Lane (1969), Morrison and Lane (1975), and Sur and Ghosh (1981) are not included in figure 15; all these calculations agree with the measurements at least in general shape.

Comparing the e^+–H_2 and e^-–H_2 results, the following statement can be made: the ratio between the positron and electron total cross sections is lower than one for energies up to 25 eV and converges to one for energies above 200 eV. In the energy range between about 30 and 200 eV, however, the positron results are higher than

the electron data. This behaviour was first reported by the Detroit group (Hoffman *et al* 1982) and attributed to inelastic scattering, which could be larger for positrons than for electrons due to the additional channel of positronium formation. This assumption is supported by the results of the calculations of Ray *et al* (1980) for positronium formation cross sections.

4. Conclusions

The comparison of our results on e^+–H_2 and e^-–H_2 total scattering with those of the groups at Wayne State University (Detroit) and University College London and other electron-only experiments shows fair agreement. The small remaining deviations will probably be resolved soon. It is significant that positron measurements with three technically quite different apparatuses agree so well over a wide energy range. This consistency demonstrated here for total scattering on H_2 is essential for accessing the accuracy of future measurements on a great variety of target molecules, some of which might only be investigated in one laboratory. It is encouraging that the measured absolute total cross sections for positrons are about as accurate as those for electrons.

Acknowledgments

The authors are deeply indebted to the people at the Bielefeld Machine Shop and Electronics Shop for their excellent work, most of it accomplished under severe time pressure. Also the staff at the Dynamitron-Tandem-Laboratorium at Bochum directed by Dipl. Phys. K Brand helped us extensively and provided friendly hospitality for the guests from Bielefeld. The small pieces of boron were cut by Mr Bluhm of Philips Corporation at Hamburg, a help we greatly appreciate. We thank Dr Jost who gave us hints about 90° energy analysers from his experience accumulated at the University of Münster. We gratefully acknowledge very useful discussions with Professors W E Kauppila and T S Stein of Wayne State University and Professor K F Canter of Brandeis University. The work has been supported by the University of Bielefeld and the Deutsche Forschungsgemeinschaft.

Appendix

The present total cross sections for positron and electron scattering on molecular hydrogen with errors as explained in § 3.3.1 in parentheses, but not including the systematic errors of § 3.3.2.

Projectile energy (eV)	Total cross section (10^{-16} cm^2)	
	e^+–H_2	e^-–H_2
6	—	13.01 (19)
7	—	12.48 (15)
8	1.12 (7)	12.02 (8)

Projectile energy (eV)	Total cross section (10^{-16} cm^2)	
	e^+–H_2	e^-–H_2
9	1.35 (7)	10.80 (14)
10	1.63 (10)	10.49 (9)
11	—	9.80 (21)
12	2.63 (4)	8.79 (6)
13	3.17 (5)	8.18 (16)
14	3.44 (7)	8.13 (12)
15	3.93 (4)	8.12 (6)
16	4.02 (5)	—
17.5	4.65 (3)	6.67 (4)
20	4.79 (4)	—
21	4.95 (5)	—
22	5.00 (5)	—
25	4.89 (3)	5.22 (3)
30	4.63 (3)	4.75 (2)
35	4.63 (4)	—
40	4.19 (5)	4.06 (3)
45	4.14 (4)	—
50	4.09 (4)	3.42 (1)
51	3.85 (4)	—
55	3.74 (4)	—
60	3.60 (3)	3.20 (2)
66	3.35 (4)	—
75	—	2.87 (2)
80	3.03 (2)	2.71 (4)
90	2.94 (3)	—
100	2.62 (2)	2.44 (4)
150	1.98 (2)	1.87 (1)
200	1.65 (2)	1.52 (2)
250	—	1.47 (1)
300	1.21 (3)	1.25 (1)
400	1.05 (2)	1.10 (3)

References

Baille P, Darewych J W and Lodge J G 1974 *Can. J. Phys.* **52** 667–77

Bhattacharyya P K and Ghosh A S 1975 *Phys. Rev.* A **12** 1881–4

Brode R B 1925 *Phys. Rev.* **25** 636–44

Brüche E 1927 *Ann. Phys., Lpz* **82** 912–46

Canter K F and Mills A P 1982 *Can. J. Phys.* **60** 551–7

Charlton M, Griffith T C, Heyland G R and Wright G L 1980 *J. Phys. B: At. Mol. Phys.* **13** L353–6

Dalba G, Fornasini P, Lazzizzera I, Ranieri G and Zecca A 1980 *J. Phys. B: At. Mol. Phys.* **13** 2839–48

Dale J M, Hulett L D and Pendyala S 1980 *Surf. Interface Anal.* **2** 199–203

Darewych J W, Baille P and Hara S 1974 *J. Phys. B: At. Mol. Phys.* **7** 2047–54

Ferch J, Raith W and Schröder K 1980 *J. Phys. B: At. Mol. Phys.* **13** 1481–90

Golden D E, Bandel H W and Salerno J A 1966 *Phys. Rev.* **146** 40–2

Griffith T C, Charlton M, Clark G, Heyland G R and Wright G L 1982 *Positron Annihilation* ed P G Coleman, S C Sharma and L M Diana (Amsterdam: North-Holland) pp 61–70

Griffith T C, Heyland G R, Lines K S and Twomey T R 1979 *Appl. Phys.* **19** 431–7

Hara S 1969 *J. Phys. Soc. Japan* **27** 1009–19

—— 1974 *J. Phys. B: At. Mol. Phys.* **7** 1748–55

Harting E and Read F H 1976 *Electrostatic Lenses* (Amsterdam: Elsevier)
Henry R J W and Lane N F 1969 *Phys. Rev.* **183** 221–31
Herrmannsfeldt W B 1973 *SLAC Report No* 166 (Electron Trajectory Program)
Hoffman K R, Dababneh M S, Hsieh Y-F, Kauppila W E, Pol V, Smart J H and Stein T S 1982 *Phys. Rev.* A **25** 1393–403
Legge G J F and Bubb I F 1961 *Nucl. Phys.* **26** 616–33
Livingston M S and Bethe H A 1937 *Rev. Mod. Phys.* **9** 245–390
Morrison M A and Lane N F 1975 *Phys. Rev.* A **12** 2361–8
Normand C E 1930 *Phys. Rev.* **35** 1217–25
Nuclear Engineering Handbook 1958 ed H Etherington (New York: McGraw Hill) § 2 p 34
Pendyala S and McGowan J W 1980 *J. Elec. Spectrosc. Rel. Phenom.* **19** 161–6
Ramsauer C and Kollath R 1930 *Ann. Phys., Lpz* **4** 91–108
Ray A, Ray P P and Saha B C 1980 *J. Phys. B: At. Mol. Phys.* **13** 4509–19
Risley J S 1972 *Rev. Sci. Instrum.* **43** 95–103
Rosenberg I J, Weiss A H and Canter K F 1980 *Phys. Rev. Lett.* **44** 1139–42
Rusch M 1925 *Phys. Z.* **26** 748–51
Simpson J A 1961 *Rev. Sci. Instrum.* **32** 1283–93
Sinapius G, Raith W and Wilson W G 1980 *J. Phys. B: At. Mol. Phys.* **13** 4079–90
Stein T S, Kauppila W E and Roellig L O 1974 *Rev. Sci. Instrum.* **45** 951–3
—— 1975 *Phys. Lett.* **51A** 327–9
Sur S and Ghosh A S 1982 *Phys. Rev.* A **25** 2519–23
Wilkins R L and Taylor H S 1967 *J. Chem. Phys.* **47** 3532–9
van Wingerden B, Wagenaar R W and de Heer F J 1980 *J. Phys. B: At. Mol. Phys.* **13** 3481–91